AND SCRATCHING PVA FILMS FOR LC-BASED BSA BIODETECTION

Cristina-Delia NECHIFOR [1 *], Marian LUȚCANU [2]

This study investigates the development of a liquid crystal (LC)-based bio-detection platform using stretched and scratched polyvinyl alcohol (PVA) films for detecting bovine serum albumin (BSA). PVA films were prepared by casting, uniaxially stretched to 12%, 17%, and 22% elongation, and scratched with P600, P800, and P1000 sandpaper grits to induce surface alignment. The nematic liquid crystal N-(4-methoxybenzylidene)-4-butylaniline (MBBA) was used to probe surface properties and BSA adsorption. Surface morphology, contact angles, and LC alignment were characterized using atomic force microscopy (AFM), contact angle measurements, and polarizing optical microscopy (POM). The contact angle of water on PVA surfaces were measured to assess wetting properties. LC cells assembled with stretched and scratched PVA films demonstrated uniform MBBA alignment, with BSA detection achieved by observing alignment disruptions in POM images. Calibration curves yielded a limit of detection (LOD) from $5.04 \times 10^{-11}\ g/mL$ *to* $1.65 \times 10^{-8}\ g/mL$*, tested at BSA concentrations ranging from* $10\ ng/mL$ *to* $1\ mg/mL$*, with sensitivity influenced by stretching elongation and sandpaper grit. These findings highlight the potential of surface-modified PVA films for sensitive LC-based bio-detection applications.*

Keywords: Polyvinyl alcohol (PVA), nematic liquid crystals, MBBA, bovine serum albumin (BSA), stretching, scratching, surface alignment, bio-detection, contact angle, polarizing optical microscopy (POM).

1. Introduction

The development of sensitive, label-free biosensing platforms has attracted considerable interest in biomedical diagnostics for enabling rapid, cost-effective, and non-invasive detection of biomolecules. Liquid crystal (LC)-based biosensors have emerged as a promising technology, exploiting the optical and anisotropic properties of LCs to transduce interfacial molecular interactions into macroscopic, visually detectable optical signals [1, 2]. LC biosensors rely on the specific interaction between an immobilized receptor and target analytes (e.g., proteins, nucleic acids, glucose), which disrupts the initially uniform LC alignment (vertical

[1]* Lecturer, Dept. of Physics, "Gheorghe Asachi" Technical University of Iași, Romania, corresponding author, e-mail cristina-delia.nechifor@academic.tuiasi.ro
[2] Eng., Dept. of Physics, "Gheorghe Asachi" Technical University of Iași, Romania, e-mail marian.lutcanu@staff.tuiasi.ro

or planar). This reorientation produces a visible change in optical texture under polarizing optical microscopy (POM), typically from dark to bright, that can be quantified via image intensity analysis [3–5]. A schematic of the detection principle is shown in Fig. 1.

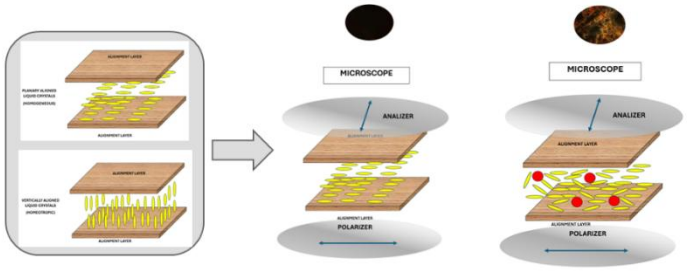

Fig. 1. Detection principle using liquid crystals (LC).

Nematic LCs such as MBBA are particularly sensitive to surface topography and chemistry, allowing label-free amplification of biomolecular binding events [6–8]. Biocompatible polymeric substrates, notably polyvinyl alcohol (PVA), offer advantages including flexibility, low cost, biodegradability, and environmental compatibility [9–11]. However, pristine PVA films typically yield disordered LC alignment, limiting biosensor sensitivity. Physical surface treatments, such as uniaxial stretching and directional mechanical scratching, can induce anisotropy and microgrooves to guide LC orientation more effectively [12–16]. Despite progress, the precise relationship between surface modification parameters and LC alignment quality remains incompletely understood, and achieving very low limits of detection (LOD) with high reproducibility on polymer substrates continues to be challenging [17–20].

The present study develops a robust LC-based platform for bovine serum albumin (BSA) detection using MBBA on surface-modified PVA films. We systematically investigate the combined effects of uniaxial stretching (12%, 17%, 22% elongation) and directional scratching with graded sandpaper (P600–P1000) on PVA film topography, wettability, and MBBA alignment quality. The specific objectives are: (1) to determine the interplay between stretching extent, scratching grit, and MBBA alignment; (2) to assess the resulting impact on sensitivity and LOD for BSA detection; (3) to establish a simple, scalable, chemical-free method for preparing PVA substrates suitable for LC biosensing.

The novelty of this work lies in the synergistic application of moderate uniaxial mechanical stretching (optimal at 17%) combined with fine directional scratching (P1000) as a purely physical, low-cost, and fully biocompatible approach to induce anisotropic surface topography on biodegradable PVA films. This method yields excellent MBBA alignment (highest $R_{Bright/Dark} = 5.39$) and outstanding BSA detection performance ($LOD \approx 50.4\ pg/mL$), among the lowest reported for POM-based LC biosensors. The findings advance the understanding of LC–

substrate interactions and provide a foundation for scalable, environmentally friendly LC-based platforms for detecting other biomolecules.

2. Materials and Methods:

2.1. Materials:

Polyvinyl alcohol (PVA, 99+% hydrolysed, average Mw = 89.000-98.000, Sigma-Aldrich) fully hydrolysed grade with limited cold-water solubility but readily dissolved at 90 °C with stirring for 12 hours to prepare 10 wt.% PVA solutions.

The nematic liquid crystals N-(4-methoxybenzylidene)-4-butylaniline (MBBA) was used as received. Bovine serum albumin (BSA, $2\ mg\ protein/ml$, $Mw = 66.5\ kDa$, Sigma-Aldrich) was diluted in phosphate-buffered saline (PBS, pH=7.4), prepared by dissolving one PBS saline tablet (Sigma-Aldrich) in 200 mL distilled water.

2.2. Film Preparation:

Polyvinyl alcohol (PVA) solutions (60 mL) were cast onto cleaned glass plates (23 cm × 23 cm) and allowed to spread freely. Films were dried in a covered enclosure at 27 °C for three days to minimize dust contamination. The resulting films were cut into standard tensile test specimens to ensure uniform mechanical behavior [21].

Films were heated to $40\ °C$ in an environmental chamber, below the glass transition temperature of PVA ($T_g = 75 - 85$ ℃), to enhance chain mobility and facilitate alignment during stretching without excessive deformation or thermal degradation. Uniaxial stretching was performed to achieve elongations (ε) of 12%, 17%, and 22%, calculated as:

$$\varepsilon(\%) = \frac{\Delta L}{L_0} \cdot 100 = \frac{L - L_0}{L_0} \cdot 100 \quad (1)$$

where ΔL is the deformation and L_0 is the original length [21]. After stretching, samples were cooled to room temperature ($25 \pm 2\ °C$) under clamped conditions for 30 min to fix the orientation. Post-release elongation was re-measured to account for minor relaxation and thickness reduction. Films were stored in a desiccator at $25 \pm 2\ °C$ in clean Petri dishes and used within 1–3 days to prevent moisture uptake. Stretched films were then scratched unidirectionally along the stretching axis using sandpaper of grades P600, P800, and P1000 (FEPA standard), with average abrasive particle diameters of approximately $25.8\ \mu m$, $21.8\ \mu m$, and $18.3\ \mu m$, respectively [22]. Scratching involved ten passes at $10\ mm/s$ under a constant force of $0.2\ N$. Loose debris was removed using compressed air (2 bar, 20 cm distance).

2.3. PVA Film Characterization:

Film thickness was measured at 10 different points using a micrometer screw gauge, with an average thickness of $80 - 90\ \mu m$. Only PVA films within this range were used in experiments due to their higher tensile strength and resistance to deformation during stretching.

Surface morphology of PVA films was analysed using Atomic Force Microscopy (AFM) with Nanosurf EasyScan 2 (Nanosurf GmbH, Langen, Germany).

Contact angles of water on PVA films were measured at room temperature (25 ± 2℃) using a KSV CAM 101 system (KSV Instruments Ltd., Helsinki, Finland) with a video camera, liquid dispenser, and drop-shape analysis software (version 3.99). The sessile drop technique was used with $3\ \mu l$ droplets. Five measurements were taken at three different regions per film surface, with an accuracy of 1°. Contact angle images were recorded after a 10 s stabilization period to ensure thermodynamic equilibrium.

2.4. Etalon LC Detection Cell Fabrication and Analysis:

Etalon LC cells were assembled using two PVA substrates with identical stretching and scratching conditions to ensure consistent surface alignment. Mylar spacers ($50\ \mu m$ thick) were placed at the edges of one substrate to define the cell gap. A thin layer ($10\ \mu L$) of MBBA was applied to one substrate at 30 °C using a micropipette to maintain the nematic phase. The second PVA substrate was aligned parallel to the stretching and scratching direction of the first to promote uniform LC alignment. The cell was sealed with UV-curable adhesive (Norland Optical Adhesive) cured under at 365 nm ($10\ mW/cm^2$) for 5 minutes. Assembled cells were cleaned with compressed air and stored in a desiccator at $25 \pm 2\ °C$.

MBBA alignment within the etalon LC cells was characterized using POM. Images were acquired at 64X magnification to evaluate the brightness uniformity and defect formation across stretching elongations and sandpaper grits based on standard error of the mean from five measurements was evaluated.

Brightness was quantified using ImageJ software (National Institutes of Health, USA). POM images were converted to grayscale, assigning each pixel an intensity value (0 for black to 255 for white). A region of interest (ROI) was defined by drawing a rectangle over the bright and dark texture areas covered by nematic liquid crystals (LCs). The average intensity (0–255) in the ROI was calculated from the histogram of the texture distribution [23]. The bright-to-dark state intensity ratio or contrast ratio ($R_{Bright/Dark}$) was determined using Equation (2):

$$R_{Bright/Dark} = \frac{I_{Bright}}{I_{Dark}} \quad (2)$$

Where: I_{Bright} is the average intensity of light transmitted in the bright state, and I_{Dark} is the average intensity of light transmitted in the dark state.

Precision was evaluated using standard error propagation based on standard error of the mean from five measurements

2.5. BSA LC Detection Platform Construction and Analysis:

The LC-based detection platform was developed to detect BSA by observing MBBA alignment changes on surface-treated PVA films. Identical PVA films were used as substrates, with one substrate immobilized with BSA at concentrations of: $C_6 = 10\,ng/mL$, $C_5 = 0.1\,\mu g/mL$, $C_4 = 1\,\mu g/mL$, $C_3 = 10\,\mu g/mL$, $C_2 = 0.1\,mg/mL$ and $C_1 = 1\,mg/mL$ prepared by diluting BSA stock solution ($2\,mg/mL$, $M_w = 66.5\,kDa$, Sigma-Aldrich) in PBS (pH 7.4).

Six 5 µL droplets of BSA solutions were deposited in a 3×2 matrix pattern on the PVA surface and incubated at 35 °C for 30 minutes in a covered Petri dish to allow adsorption. Unbound BSA was rinsed with PBS, and films were dried with compressed air. Control regions on the same films were left untreated. Optical microscopy confirmed the BSA adsorption.

LC cells for BSA detection were assembled as described in Section 2.4, with one substrate containing immobilized BSA. MBBA response to BSA was evaluated using POM at 32× magnification, comparing alignment in BSA-immobilized and control regions. Alignment disruptions (uniform to disordered textures, defect formation) indicated BSA presence.

ImageJ software was used to quantify the mean grey intensity in POM images, reflecting LC alignment changes. Five regions per sample were analysed across three cells for reproducibility. Calibration curves plotted net mean grey intensity against the logarithm of BSA concentration, with the limit of detection (LOD) determined as the concentration where intensity reached zero (no LC alignment disruption). The net mean grey intensity ($\Delta I = I_{BSA} - I_{Control}$) was used as the analytical signal to construct semi-log calibration curves. LOD was determined by extrapolating the linear regression to $\Delta I = 0$ (baseline return), equivalent to the IUPAC 3σ criterion given the near-zero net blank signal and variability captured from $n = 5$ replicate control measurements. Sensitivity was assessed by comparing stretching elongations (12%, 17%, 22%) and sandpaper grits (P600, P800, P1000) to identify optimal conditions for LC alignment contrast.

3. Results and Discussion

3.1. PVA Film Characterization:

The surface topography of polyvinyl alcohol (PVA) films subjected to varying degrees of uniaxial stretching (0%, 12%, 17%, and 22%) was investigated using non-contact atomic force microscopy (AFM). Fig. 2 presents the AFM images and key roughness parameters, including average roughness (Sa), root mean square roughness (Sq), maximum peak height (Sp), maximum valley depth (Sv), and total

surface height (Sy), measured to elucidate the effects of mechanical stretching on the surface morphology of the films, as summarized in Table 1.

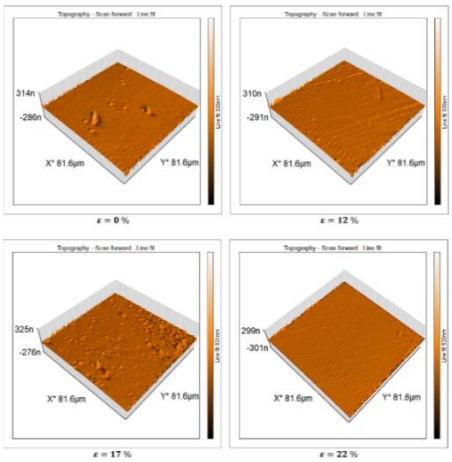

Fig. 2. AFM images of PVA films subjected to varying degrees of uniaxial stretching (0%, 12%, 17%, and 22%).

Table 1.

The AFM images and key roughness parameters of PVA films subjected to varying degrees of uniaxial stretching (0%, 12%, 17%, and 22%).

Stretching Elongation, $\varepsilon(\%)$	$S_a(nm)$	$S_q(nm)$	$S_p(nm)$	$S_v(nm)$	$S_y(nm)$
0%	28.81	36.52	376.22	-133.58	509.81
12%	31.14	37.43	301.83	-123.89	425.72
17%	31.88	40.06	369.68	-177.17	546.86
22%	28.19	35.67	383.49	-109.79	493.27

Unstretched (0% strain) PVA films exhibited moderate surface heterogeneity, with roughness parameters $Sa = 28.81\,nm, Sq = 36.52\,nm, Sp = 376.22\,nm, Sv = -133.58\,nm$, and $Sy = 509.81\,nm$, reflecting significant topographic variations. At 12% strain, slight increases occurred in Sa $(31.14\,nm)$ and Sq $(37.43\,nm)$, accompanied by reductions in peak height Sp $(301.83\,nm)$, valley depth Sv $(-123.89\,nm)$, and peak-to-valley height Sy $(425.72\,nm)$. This indicates initial smoothing induced by polymer chain alignment, which diminishes extreme topographic features. Roughness peaked at 17% strain, with $Sa = 31.88\,nm, Sq = 40.06\,nm$, and $Sy = 546.86\,nm$, driven by deepened valleys $(Sv = -177.17\,nm)$ and elevated peaks $(Sp = 369.68\,nm)$. These changes suggest the formation of pronounced stress-induced defects (microcracks or localized depressions) when mechanical loading exceeds the threshold for uniform deformation, as Sq is particularly sensitive to outlier height variations. At 22% strain, the surface partially recovered uniformity, with Sa decreasing to $28.19\,nm, Sq$ to $35.67\,nm$, and Sy to $493.27\,nm$, while Sp

increased slightly ($383.49\,nm$) and Sv became shallower ($-109.79\,nm$). This stabilization likely results from maximized chain alignment and/or stress relaxation at higher elongations, mitigating deep valleys. Overall, surface topography evolves non-linearly with strain: mild stretching (12%) promotes smoothing via chain reorientation, moderate stretching (17%) generates significant defects from localized stress concentrations, and higher stretching (22%) leads to partial recovery through enhanced alignment and relaxation. These observations underscore the complex interplay between polymer chain reorganization and the nucleation/relaxation of mechanical defects during uniaxial deformation.

The AFM images of PVA films subjected to varying degrees of uniaxial stretching (0%, 12%, 17%, and 22%) then scratched with sandpaper (P 600, P 800 and P1000) are presented in Fig. 3. The key roughness parameters: average roughness (Sa), root mean square roughness (Sq), maximum peak height (Sp), maximum valley depth (Sv), and total surface height (Sy) are listed in Table 2.

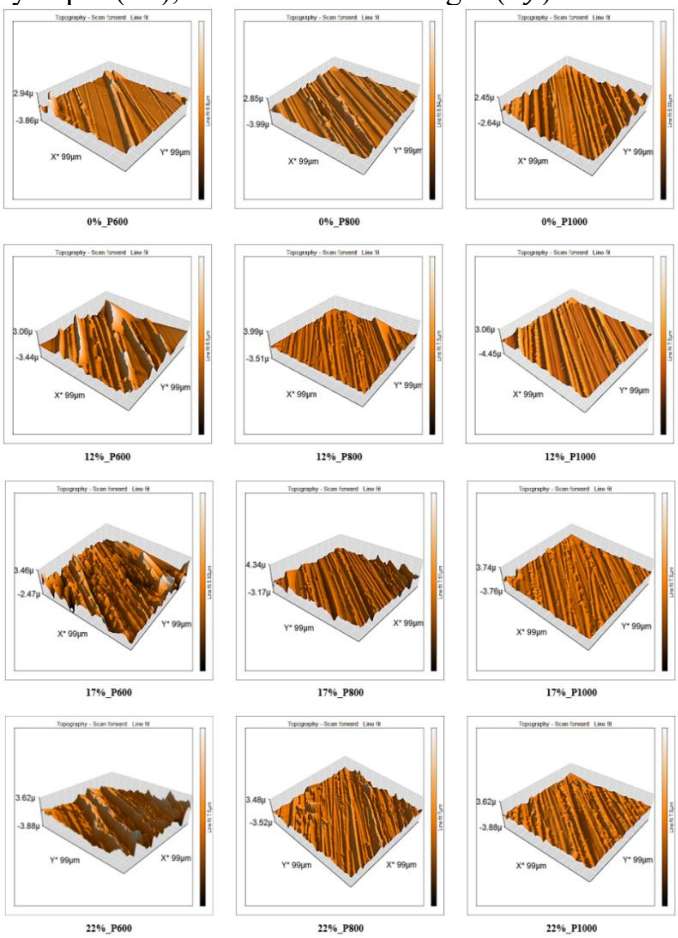

Fig. 3. AFM images of PVA films subjected to varying degrees of uniaxial stretching (0%, 12%, 17%, and 22%) then scratched with sandpaper (P600, P800, and P1000).

Fig. 3 and Table 2 reveal that scratching introduces significant roughness, with coarser grits (P600) producing the most pronounced topographic features (high $Sy = 4480.2\,nm$). Finer grits (P1000) create more uniform surfaces with consistent microgrooves and less disruption ($Sy = 3447.1\,nm$). High Sy values across grits indicate scratching dominates the isotropic PVA surface, yielding a highly textured topography.

Table 2.

The AFM images and key roughness parameters of PVA films subjected to varying degrees of uniaxial stretching (0%, 12%, 17%, and 22%) then scratched with sandpaper (P600, P800 and P1000).

Sample	$Sa(nm)$	$Sq(nm)$	$Sp(nm)$	$Sv(nm)$	$Sy(nm)$
0%_P600	245.39	389.60	3207.8	-1272.3	4480.2
0%_P800	247.71	323.52	1309.0	-2053.5	3362.5
0%_P1000	230.96	301.14	2070.7	-1376.4	3447.1
12%_P600	611.71	798.39	3127.7	-2422.8	5550.5
12%_P800	199.03	275.02	3035.4	-767.54	3802.9
12%_P1000	168.00	231.88	1253.5	-934.36	2187.9
17%_P600	571.8	753.24	3779.0	-2771.1	6550.1
17%_P800	262.03	386.39	1744.7	-1934.0	3678.7
17%_P1000	124.75	173.51	1138.7	-1309.5	2448.3
22%_P600	702.05	873.84	3739.8	-3367.1	7106.9
22%_P800	276.29	376.47	1827.0	-1331.7	3158.7
22%_P1000	231.34	304.26	1432.3	-1176.5	2608.8

Stretching at 12% elongation aligns polymer chains, forming an anisotropic base that interacts variably with grits. P600 exacerbates roughness ($Sa = 611.71\,nm, Sy = 5550.5\,nm$), while P1000 yields a smoother, uniform surface ($Sa = 168\,nm,\ Sy = 2187.9\,nm$) with aligned microgrooves along the stretching direction. Increased stretching stress at 17% elongation (peaking roughness in Table 1) amplifies coarse scratching (P600: $Sy = 6550.1\,nm$, highest among 17% samples). Finer grits (P800, P1000) produce smoother surfaces, with P1000 most uniform topography ($Sa = 124.75\,nm, Sy = 2448.3\,nm$).

Stabilized topography (Table 1) with P600 scratching results in highest overall roughness ($Sa = 702.05\,nm,\ Sy = 7106.9\,nm$) at 22% elongation, featuring excessive groove depth and irregularity. P1000 provides the most uniform surface ($Sa = 231.34\,nm, Sy = 2608.8\,nm$).

Across stretching levels, P600 yields highest roughness (Sa, Sq, Sy) with deep valleys (Sv) and high peaks (Sp), indicating disruption that may cause non-uniform LC alignment and reduced BSA detection sensitivity due to irregular microgrooves. Finer grits (P800, P1000) lower roughness, with P1000 optimal (lowest Sa, Sq, Sy), offering consistent microgrooves for enhanced LC alignment, higher POM contrast ratio ($R_{Bright/Dark}$), and improved BSA sensitivity.

Stretching alone (Table 1) shows non-linear roughness, peaking at 17% due to stress-induced defects. Combined with scratching, peak roughness shifts to 22% with P600 ($Sy = 7106.9\,nm$), as maximized chain alignment amplifies coarse grit effects. Moderate stretching (12%, 17%) with P1000 minimizes roughness ($Sa = 168\,nm$ at 12%, $124.75\,nm$ at 17%), creating ideal conditions for LC alignment. Scratching elevates parameters by orders of magnitude (Sy: $\sim 500\,nm$ in Table 1 to $2000 - 7100\,nm$ in Table 2), dominating topography with LC-guiding microgrooves. The Table 1 trend (17% peak) is modified, with scratching enhancing alignment effects at higher strains, especially coarse grits.

Contact angles of water on pristine and processed PVA films are given in table 3. Values are mean ± standard error (n=5).

Table 3.

Water contact angles on pristine and processed PVA films.

Sample	Water Contact Angle,θ_w (degree)
0 %	60.80±0.70
0 %_P600	49.27±2.98
0 %_P800	42.27±3.18
0 %_P1000	43.80±1.12
12 %	55.70±0.70
12 %_P600	45.57±2.42
12%_P800	47.60±0.40
12%_P1000	44.81±1.50
17%	66.75±0.14
17 %_P600	43.85±5.97
17 %_P800	45.15±0.66
17 %_P1000	35.10±2.87
22 %	60.50±0.70
22 %_P600	50.50±0.53
22 %_P800	49.20±4.95
22 %_P1000	55.21±0.10

Table 3 shows that pristine PVA films have a contact angle (θ_w) of $60.80° \pm 0.70°$, indicating moderate hydrophilicity due to hydroxyl groups and smooth topography ($Sa = 28.81\,nm$, Table 1). Stretching to 12% elongation reduces θ_w to $55.70° \pm 0.70°$, enhancing hydrophilicity as smoother surfaces ($Sy = 425.72\,nm$) and aligned polymer chains expose more hydroxyl groups. At 17% elongation, θ_w peaks at $66.75° \pm 0.14°$, reflecting increased hydrophobicity due to peak roughness ($Sa = 31.88\,nm, Sy = 546.86\,nm$) and stress-induced defects like microcracks that trap air or limit hydroxyl group access. At 22% elongation, θ_w decreases to $60.50° \pm 0.70°$, nearing pristine levels, with stabilized topography ($Sa = 28.19\,nm, Sy = 493.27\,nm$) indicating balanced chain alignment and reduced defects. Scratching pristine PVA films reduces θ_w by

$11 - 18°$, enhancing hydrophilicity. Increased roughness ($Sy = 4480.2\,nm$ for P600, Table 2) and microgrooves promote water spreading, with finer grits (P800, P1000) yielding lower θ_w due to uniform, shallower grooves ($Sy = 3362.5 - 3447.1\,nm$). For 12% elongated films, scratching lowers θ_w by $8 - 11°$, with P1000 producing the smoothest scratched surface ($Sa = 168\,nm, Sy = 2187.9\,nm$) and highest hydrophilicity. The lowest θ_w (35.10°) occurs at 17% elongation with P1000, reflecting optimal hydrophilicity from aligned microgrooves and smoothest scratched surface ($Sa = 124.75\,nm, Sy = 2448.3\,nm$). However, P600 at 17% shows high variability ($\pm 5.97°$) due to irregular, deep grooves ($Sy = 6550.1\,nm$). At 22% elongation, scratched films have higher θ_w (55.21° for P1000) despite similar roughness ($Sa = 231.34\,nm, Sy = 2608.8\,nm$), suggesting excessive chain alignment reduces polar group accessibility.

Stretching induces non-linear wettability changes: initial stretching (12%) enhances hydrophilicity via chain alignment and smoother surfaces, while 17% increases hydrophobicity due to roughness and defects. Scratching consistently enhances hydrophilicity by increasing roughness and forming microgrooves, with finer grits (P1000) producing the lowest θ_w at 17% elongation due to synergistic chain alignment and uniform grooves. Surface texturing from scratching dominates wettability, significantly reducing θ_w across all stretching levels compared to stretched-only films.

3.2. Etalon LC Detection Cell and BSA LC Detection Platform Construction and Analysis:

The alignment of MBBA molecules in etalon LC cells was characterized using polarizing optical microscopy (POM) for PVA films stretched at 0%, 12%, 17%, and 22% elongation and scratched with P600, P800, and P1000 sandpaper grits. Contrast ratios ($R_{Bright/Dark}$), calculated as the ratio of bright to dark state intensities (Equation 2), quantify MBBA alignment uniformity, with higher ratios indicating better alignment critical for sensitive BSA detection. Results are presented in Table 4 and Fig. 4 (POM images for 17% elongation).

Pristine films showed poor alignment ($R_{Bright/Dark} = 1.28 \pm 0.52$) due to isotropic surfaces ($Sa = 28.81\,nm,\ Sy = 509.81\,nm$, Table 1; $\theta_w = 60.80° \pm 0.70°$, Table 3). Scratching improved alignment, with P800 yielding the highest contrast ratio (3.63 ± 1.02) due to uniform grooves ($Sa = 247.71\,nm, Sy = 3362.5\,nm$) and enhanced hydrophilicity ($\theta_w = 42.27° \pm 3.18°$), while P600 ($2.02 \pm 0.72$) and P1000 ($1.45 \pm 1.3$) showed lower ratios due to irregular or insufficient grooves.

The stretched films at 12% elongation possess a minor improvement in alignment without scratching ($R_{Bright/Dark} = 1.46 \pm 0.65$; $Sa = 31.14\,nm$, $\theta_w = 55.70°$). P1000 scratching yielded the highest ratio (2.94 ± 0.95) with the

smoothest scratched surface ($Sa = 168.00\,nm, Sy = 2187.9\,nm$) and high hydrophilicity ($\theta_w = 44.81° \pm 1.50°$), while P600 ($1.97 \pm 0.84$) and P800 ($2.31 \pm 1.25$) showed moderate alignment. When films were stretched at 17% elongation, the highest contrast ratio (5.39 ± 1.45) was achieved with P1000 scratching ($Sa = 124.75\,nm,\ Sy = 2448.3\,nm;\ \theta_w = 35.10° \pm 2.87°$), indicating optimal MBBA alignment due to uniform microgrooves and maximum hydrophilicity. P600 (2.85 ± 1.75) and P800 (1.94 ± 0.43) showed lower ratios due to coarser, less uniform grooves. POM images (Fig. 4) confirm uniform bright textures for 17%_P1000, with defects in P600 and P800 samples.

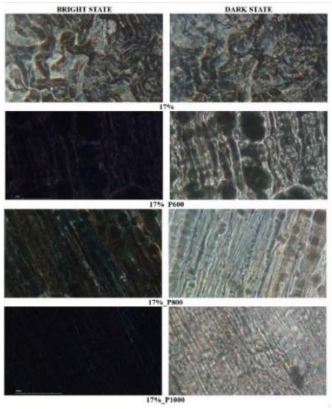

Fig. 4. POM images of etalon LC cells obtained using PVA films stretched at 17% elongation.

Table 4.

Contrast Ratios ($R_{Bright/Dark}$) of POM Images for MBBA molecules within the etalon LC cells

Sample	Contrast Ratios ($R_{Bright/Dark}$)
0 %	1.28±0.52
0 %_P600	2.02±0.72
0 %_P800	3.63±1.02
0 %_P1000	1.45±1.30
12 %	1.46±0.65
12 %_P600	1.97±0.84
12%_P800	2.31±1.25
12%_P1000	2.94±0.95
17%	1.87±0.70
17 %_P600	2.85±1.75
17 %_P800	1.94±0.43
17 %_P1000	5.39±1.45
22 %	2.83±0.82
22 %_P600	2.27±0.35
22 %_P800	2.95±0.74
22 %_P1000	1.58±0.65

The non-scratched films (stretched at 22% elongation) showed good alignment ($R_{Bright/Dark} = 2.83 \pm 0.82$; $Sa = 28.19\,nm$, $\theta_w = 60.50°$), but P1000 scratching reduced alignment (1.58 ± 0.65) despite uniform topography, likely due to reduced hydrophilicity. P800 (2.95 ± 0.74) and P600 (2.27 ± 0.35) showed moderate alignment.

The 17%_P1000 combination has the highest $R_{Bright/Dark}$, reflecting uniform LC alignment, enhancing sensitivity to BSA-induced disruptions. Finer scratching (P1000) at 17% elongation produces uniform microgrooves and high hydrophilicity, maximizing MBBA anchoring. Coarser grits (P600) increase roughness, reducing alignment uniformity and sensitivity. Excessive stretching (22%) with P1000 lowers hydrophilicity, limiting alignment. These findings confirm that 17% elongation with P1000 scratching provides a scalable, sensitive LC-based platform for BSA detection, leveraging synergistic surface topography and wettability.

3.3. BSA LC Detection Platform Construction and Analysis

The LC-based detection platform was developed to quantify bovine serum albumin (BSA) by observing MBBA alignment disruptions on surface-modified PVA films, as detailed in Section 2.5. PVA substrates, prepared with uniaxial stretching (0%, 12%, 17%, 22%) and scratched with P600, P800, and P1000 sandpaper grits (Section 2.2), were immobilized with BSA at concentrations of $10\,ng/mL$ to $1\,mg/mL$. LC cells were assembled with one BSA-immobilized substrate and one untreated substrate, using 50 μm Mylar spacers and MBBA in the nematic phase (Section 2.4). Polarizing optical microscopy (POM) images (Fig.5), calibration lines (Fig.6), and limits of detection (LODs) (Table 5) were analysed to evaluate sensitivity and detection performance.

The biosensing mechanism relies on the specific adsorption of BSA onto the PVA surface, which perturbs the uniform alignment of MBBA molecules. BSA adsorbs via hydrogen bonding with PVA hydroxyl groups and hydrophobic interactions, increasing surface roughness locally and altering the anchoring energy. This induces a reorientation of MBBA from uniform (dark POM texture in crossed polarizers) to disordered/tilted (bright, defect-rich texture), with the degree of disruption proportional to BSA surface coverage [8,10].

Fig. 5 presents the POM images and quantitative analysis (mean grey intensity) of BSA LC cells obtained using 17%_P1000 sample with immobilized BSA at concentrations of 10 ng/mL to 1 mg/mL.

Fig.6 shows the calibration lines of the sample stretched at 17% elongation and scratched with P600, P800, and P1000 sandpaper grits. Calibration lines were generated by plotting net mean grey intensity from POM images, quantified using ImageJ software, against the logarithm of BSA concentration. The positive slopes confirmed that higher BSA concentration increases intensity (more disruption); the

limit of detection (LOD) was determined as the extrapolated concentration where net intensity returned to the control baseline (zero net disruption beyond noise). Table 5 presents the slopes, R^2 values, and LODs for each condition.

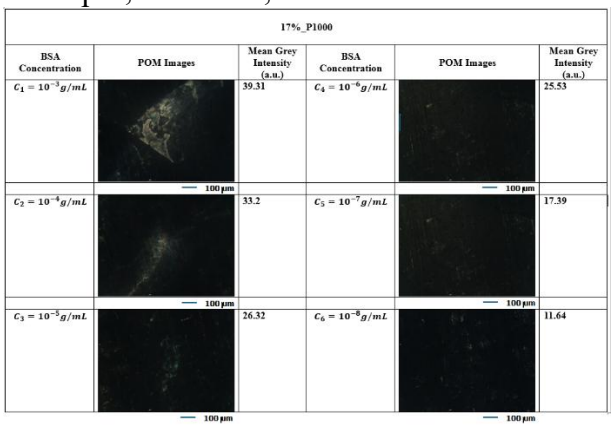

Fig.5. POM images of BSA LC cells obtained using 17%_P1000 sample with immobilized BSA, showing increasing brightness (higher mean grey intensity) with BSA concentration.

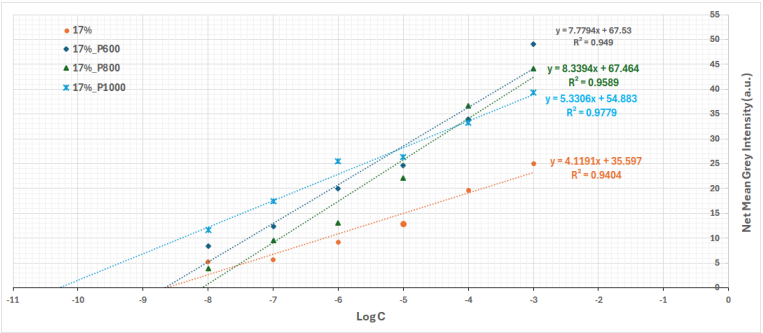

Fig. 6. Calibration lines of BSA LC cells obtained using samples stretched at 17% elongation and scratched with P600, P800, and P1000 sandpaper grits with various concentrations of immobilized BSA.

The slope, representing sensitivity (mean grey intensity change per log [BSA concentration] expressed as $a.u./log\ (g/mL)$, was highest for 0%_P600 (9.22) and 12%_P1000 (8.96), indicating strong responsiveness to BSA concentration changes. However, 17%_P1000, with a slope of 5.33 and the highest $R_{Bright/Dark}$ (5.39), achieved the lowest LOD (5.04×10^{-11} g/mL), suggesting that sensitivity alone does not determine detection performance. This reflects the balance between uniform MBBA alignment and effective BSA-induced disruptions. Lower slopes, such as 4.12 for 17% (unscratched) and 4.91 for 22%_P800, correlated with higher LODs (2.20×10^{-9} g/mL and 4.48×10^{-9} g/mL, respectively), indicating reduced sensitivity due to less uniform alignment ($R_{Bright/Dark} = 1.87$ and 2.95, Table 4). R^2 values, ranging from 0.9178 to

0.9921, confirmed good linear fits across all conditions, with 22% (unscratched) showing the highest linearity ($R^2 = 0.9921$). High R^2 values indicate reliable calibration for quantifying BSA concentrations, supporting the reproducibility of the proposed platform.

Table 5.

Sensitivity and LOD for BSA Detection on Surface-Modified PVA Films

Sample	Calibration Line		LOD (g/ml)
	Slope	R^2 value	
0%	6.87	0.9387	1.06×10^{-8}
0%_P600	9.22	0.9806	4.17×10^{-9}
0%_P800	6.33	0.9864	7.81×10^{-10}
0%_P1000	7.25	0.9255	1.65×10^{-8}
12%	5.70	0.9178	7.74×10^{-9}
12%_P600	6.67	0.9862	3.16×10^{-9}
12%_P800	7.91	0.9551	3.49×10^{-9}
12%_P1000	8.96	0.9553	1.14×10^{-10}
17%	4.12	0.9404	2.20×10^{-9}
17%_P600	7.78	0.9490	2.09×10^{-9}
17%_P800	8.34	0.9589	8.13×10^{-9}
17%_P1000	5.33	0.9779	5.04×10^{-11}
22%	6.77	0.9921	1.40×10^{-9}
22%_P600	7.15	0.9449	2.30×10^{-9}
22%_P800	4.91	0.9831	4.48×10^{-9}
22%_P1000	5.47	0.9603	9.95×10^{-9}

The lowest LOD ($5.04 \times 10^{-11}\ g/mL$, or $50.4\ pg/mL$) was achieved for 17%_P1000, reflecting its superior detection capability due to uniform microgrooves ($Sa = 124.75\ nm$), high hydrophilicity ($\theta_w = 35.10°$), and optimal MBBA alignment ($R_{Bright/Dark} = 5.39$). This LOD highlights the ability of the platform to detect trace BSA levels, competitive with advanced biosensing methods. Higher LODs for 0%_P1000 ($16.5\ ng/mL$) and 22%_P1000 ($9.95\ ng/mL$) reflect suboptimal alignment ($R_{Bright/Dark} = 1.45$ and 1.58) and surface properties, reducing sensitivity to low BSA concentrations.

4. Conclusions

This study successfully developed a label-free liquid crystal (LC)-based biosensing platform using MBBA on uniaxially stretched and mechanically scratched polyvinyl alcohol (PVA) films for sensitive detection of bovine serum albumin (BSA). Systematic investigation of surface modifications, uniaxial stretching (0%, 12%, 17%, 22% elongation) combined with directional scratching using P600, P800, and P1000 sandpaper, demonstrated their profound effects on

surface topography, wettability, MBBA alignment, and biosensing performance. Atomic force microscopy revealed that stretching induces non-linear roughness increases, peaking at 17% elongation ($Sa = 31.88\,nm, Sy = 546.86\,nm$), while scratching markedly enhances roughness (Sy up to $7106.9\,nm$ for 22%_$P600$). Finer grits (P1000) at moderate stretching (12–17%) produced uniform microgrooves with optimal smoothness ($Sa = 168.00\,nm$ and $124.75\,nm$, respectively), ideal for guiding LC orientation. Contact angle data confirmed enhanced hydrophilicity from scratching, with the 17%_P1000 condition yielding the lowest water contact angle ($35.10° \pm 2.87°$), favoring polar MBBA anchoring. POM analysis of LC cells showed superior alignment for 17%_P1000 films, evidenced by the highest bright/dark contrast ratio ($R_{Bright/Dark} = 5.39 \pm 1.45$). Coarser grits or excessive stretching degraded uniformity ($R_{Bright/Dark} \approx 2.02 - 2.27$), reducing sensitivity. BSA detection performance was highest under the 17%_P1000 condition, achieving a limit of detection (LOD) of $5.04 \times 10^{-11}\,g/mL$ ($50.4\,pg/mL$) with a moderate calibration slope (5.33) and excellent linearity ($R^2 = 0.9178 - 0.9921$). This LOD outperforms many reported POM-based LC biosensors on polymer substrates. Suboptimal alignment in unstretched ($LOD = 16.5\,ng/mL$) or over-stretched ($9.95\,ng/mL$) conditions correlated with poorer performance. These results validate the hypothesis that synergistic, chemical-free physical modifications (moderate stretching and fine scratching) optimize PVA surface anisotropy and wettability for enhanced MBBA alignment and amplified biomolecular disruption signals. The approach offers a simple, scalable, low-cost, and biocompatible alternative to conventional rubbing or chemical treatments, enabling environmentally friendly, disposable LC biosensors. Short-term stability was confirmed (stable POM contrast after 1–3 days in desiccator and during assembly), with preliminary dry storage showing no degradation over 1–2 weeks. However, long-term durability remains unquantified, and the PVA hydrophilicity may cause swelling or groove erosion in prolonged wet conditions.

Future work will prioritize quantitative durability assessments and protective modifications. Expanding to other analytes and additional treatments will further reduce LODs and broaden biomedical and environmental applications, leveraging the demonstrated synergy of topography and wettability in LC–substrate interactions.

REFERENCES

[1] Qu, R.; Guoqiang Li, G.; 2022, Overview of Liquid Crystal Biosensors: From Basic Theory to Advanced Applications**,** *Biosensors* 2022, *12*(4), 205; https://doi.org/10.3390/bios12040205

[2] Gupta, V.K.; Skaife, J.J.; Dubrovsky, T.B.; Abbott, N.L.; Optical amplification of ligand-receptor binding using liquid crystals, Science 279(5359):2077, 1998, DOI: 10.1126/science.279.5359.2077

[3] Zhan, X.; Liu, Y.; Yang, K.-L. and Luo, D.; State-of-the-Art Development in Liquid Crystal Biochemical Sensors, *Biosensors* **2022**, *12*(8), 577; https://doi.org/10.3390/bios12080577

[4] Chang, T.-K.; Lee, M.-J. and Lee, W, Quantitative Biosensing Based on a Liquid Crystal Marginally Aligned by the PVA/DMOAP Composite for Optical Signal Amplification, *Biosensors* **2022**, *12*(4), 218; https://doi.org/10.3390/bios12040218
[5] Cui, Y.; Zola, R. S.; Yang, Y.-C.; Yang, D.-K.; Alignment layers with variable anchoring strengths from Polyvinyl Alcohol, *J. Appl. Phys.* 111, 063520 (2012), https://doi.org/10.1063/1.3697680
[6] Gupta. V. K.; Skaife, J. J.; Dubrovsky. T.; Abbott, N. L. (1998). Optical amplification of ligand–receptor binding using liquid crystals, Science, 279(5359), 2077–2080, https://doi.org/10.1126/science.279.5359.2077
[7] Kim, W.; Kim, D. S.; Yoon, D. K.; Surface-induced orientation of liquid crystal phases, Giant, 19, August 2024, 100324, https://doi.org/10.1016/j.giant.2024.100324
[8] Xue, C.-Y., and Yang, K.-L. (2008), Dark-to-bright optical responses of liquid crystals supported on solid surfaces decorated with proteins , Langmuir 24(2):563-567, https://doi.org/10.1021/la7026626
[9] Paradossi,G.; Cavalieri, F.; Chiessi, E.; Spagnoli, C.; Cowman, M. K.; *Poly(vinyl alcohol) as versatile biomaterial for potential biomedical applications*, 2003, J. Mater. Sci. Mater. Med.14(8):687-691, https://doi.org/10.1023/A:1024907615244
[10] Nechifor, C.-D.; Postolache, M.; Albu, R. M.; Barzic, A. I.; Dorohoi, D.-O.,2019, *Induced birefringence of rubbed and stretched polyvinyl alcohol foils as alignment layers for nematic molecules*, Polym. Adv. Technol. 30 (8), 2143-2152, https://doi.org/10.1002/pat.4647
[11] Baker, M. I.; Walsh, S. P.; Schwartz, Z.; Boyan, B. D., 2012*, A review of polyvinyl alcohol and its uses in cartilage and orthopedic applications,* J Biomed. Mater. Res. B Appl. Biomater. 100(5):1451-1457, https://doi.org/10.1002/jbm.b.32694
[12] Stöhr, J.; Samant, M. G.; Cossy-Favre, A.; Díaz, J.; Momoi, Y.; Odahara, S.; Nagata, T.; *Microscopic Origin of Liquid Crystal Alignment on Rubbed Polymer Surfaces,* Macromolecules 1998, 31, 6, 1942–1946, https://doi.org/10.1021/ma9711708
[13] Aoyama, H., Yamazaki, Y., Matsuura, N., Mada, H., & Kobayashi, S. (1981). Alignment of Liquid Crystals on the Stretched Polymer Films. *Molecular Crystals and Liquid Crystals*, *72*(4), 127–132. https://doi.org/10.1080/01406568108084048
[14] Mamonova, A. V.; Gorkunov, M. V.; Kasyanova, I. V.; Artemov, V. V.; Palto, S. P., 2020, *Controlling liquid crystal alignment by micro-patterned substrates,* J. Phys.: Conf. Ser. **1461** 012089, https://doi.org/10.1088/1742-6596/1461/1/012089
[15] Babakhanova, G.; Lavrentovich, O. D., 2019, The Techniques of Surface Alignment of Liquid Crystals, Springer Proceedings in Physics Vol. 223; ISSN 0930-8989, https://doi.org/10.1007/978-3-030-21755-6_7
[16] Barzic, A.I.; Albu, R.M.; Stoica,I.; Nechifor, C.-D.; Avadanei, M. I.; Dimitriu, D.G; Dorohoi, D.-O., *Birefringent polyvinyl alcohol layers as retardation components for display devices*, **2024**, Polym. Adv. Technol. 35(1), e6196, https://doi.org/10.1002/pat.6196
[17] Wang H, Xu T, Fu Y, Wang Z, Leeson MS, Jiang J, Liu T. Liquid Crystal Biosensors: Principles, Structure and Applications. Biosensors (Basel). 2022 Aug 14;12(8):639. https://doi.org/10.3390/bios12080639 .
[18] Carter, D. C.; and Ho, J. X. (1994), Structure of serum albumin, Advances in Protein Chemistry, 45, 153–203, https://doi.org/10.1016/S0065-3233(08)60640-3
[19] Luan, C.; Luan, H.; Luo, D. Application and Technique of Liquid Crystal-Based Biosensors. *Micromachines* **2020**, *11*, 176. https://doi.org/10.3390/mi11020176
[20] Lee, B.W.; Clark, N.A.; **2001**, Alignment of liquid crystals with patterned isotropic surfaces, Science. 291(5513):2576-80, https://doi.org/10.1126/science.291.5513.2576
[21] Brent Strong A (1999) Plastics: Materials and Processing. Prentice–Hall, New York
[22] Nguyen, H.N.G.; Zhao, C.-F.; Millet, O.; Selvadurai, A.P.S.*; Effects of surface roughness on liquid bridge capillarity and droplet wetting*, Powder Technology 378 (2021), 487–496, https://doi.org/10.1016/j.powtec.2020.10.016
[23] ***Rasband WS (2012) ImageJ User Guide. National Institutes of Health. https://imagej.nih.gov/ij/docs/guide/